Supplementary information

Dispersion-free inertial focusing (DIF) for high-yield polydisperse micro-particles filtration and analysis

*Kelvin C. M. Lee[1,2], Bob M. F. Chung[1,2], Dickson M. D. Siu,[1,2], Sam C. K. Ho[1,2], Daniel K. H. Ng[1], Kevin K. Tsia[1,2]**

1. *The University of Hong Kong, Pokfulam road, Hong Kong, HKSAR*
2. *Advanced Biomedical Instrumentation Centre, Hong Kong Science Park, Shatin, New Territories, Hong Kong*

** Corresponding author, e-mail: tsia@hku.hk*

Table of content

Video S3: Evolution of cross-section particle distribution in DIF system (HAR symmetric orifice channel then HAR rectangular channel)

Video S4: Evolution of cross-section particle distribution in revsered DIF system (HAR rectangular channel then HAR symmetric orifice channel)

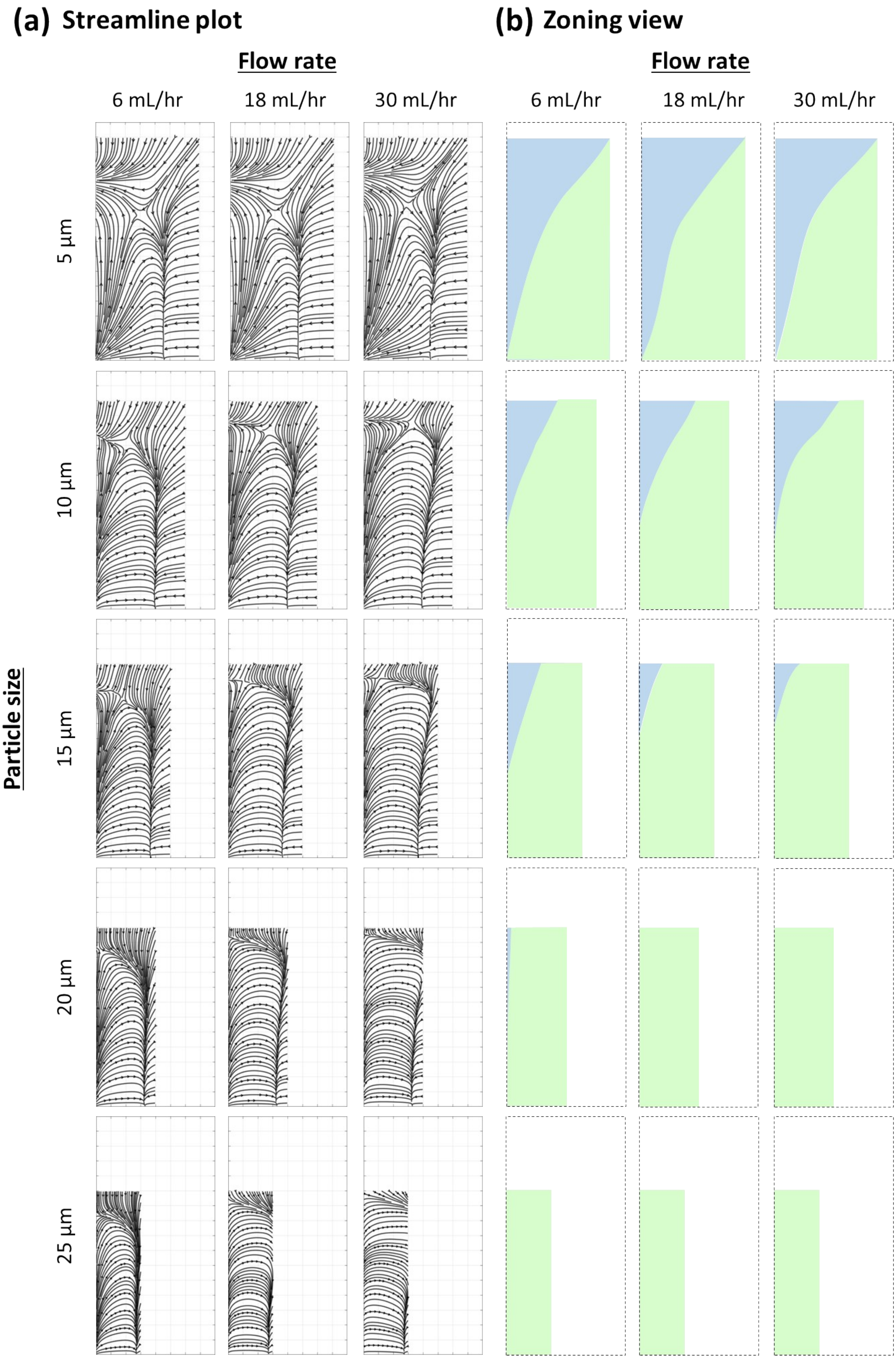

Figure S1. Inertial force field of a HAR rectangular channel by DNS. (a) Streamline plot of force field at various conditions. (b) The corresponding zoning view.

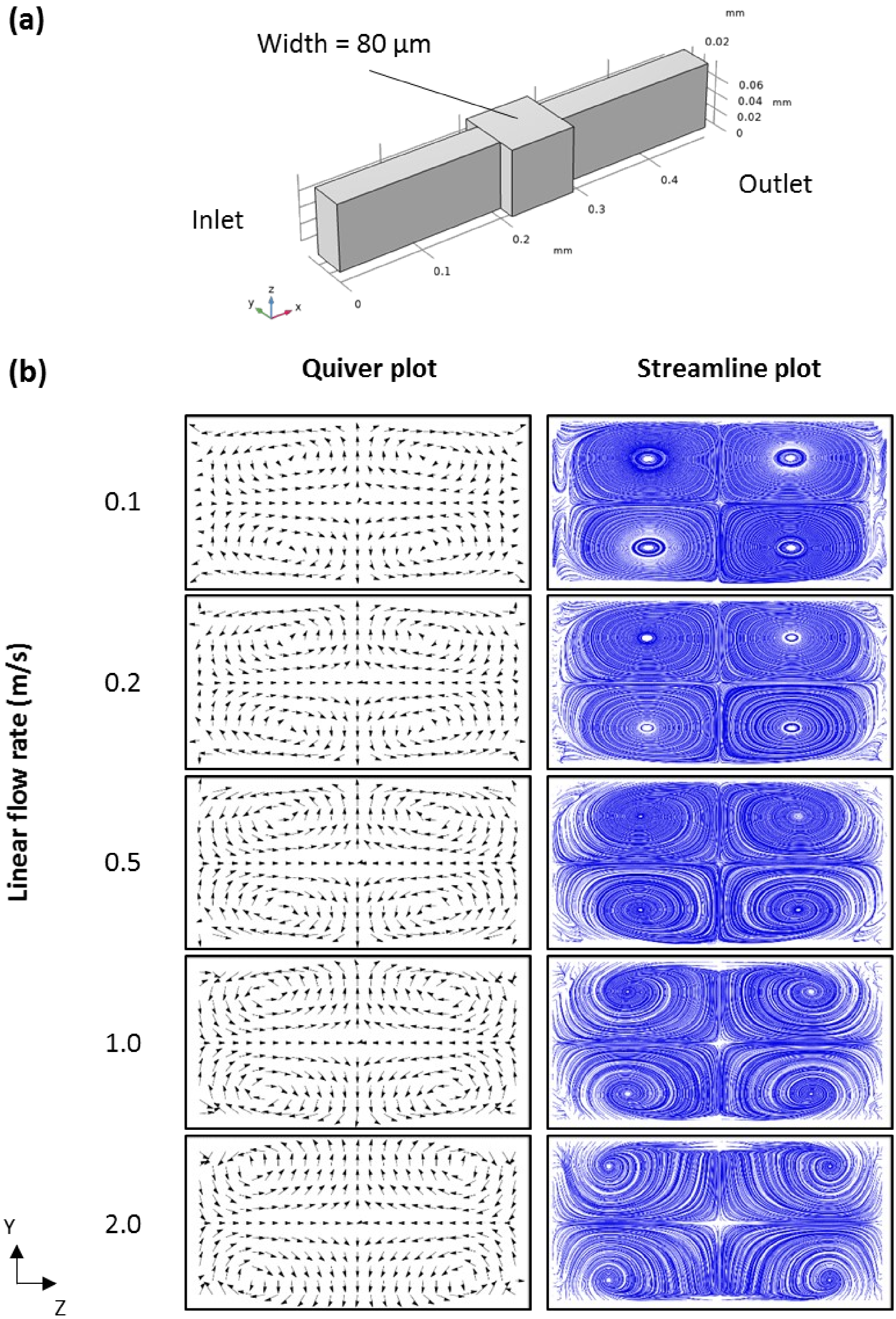

Figure S2. Simulation result of secondary flows induced by a HAR symmetric orifice. (a) CFD Model. (b) Quiver and streamline plots of the secondary flow.

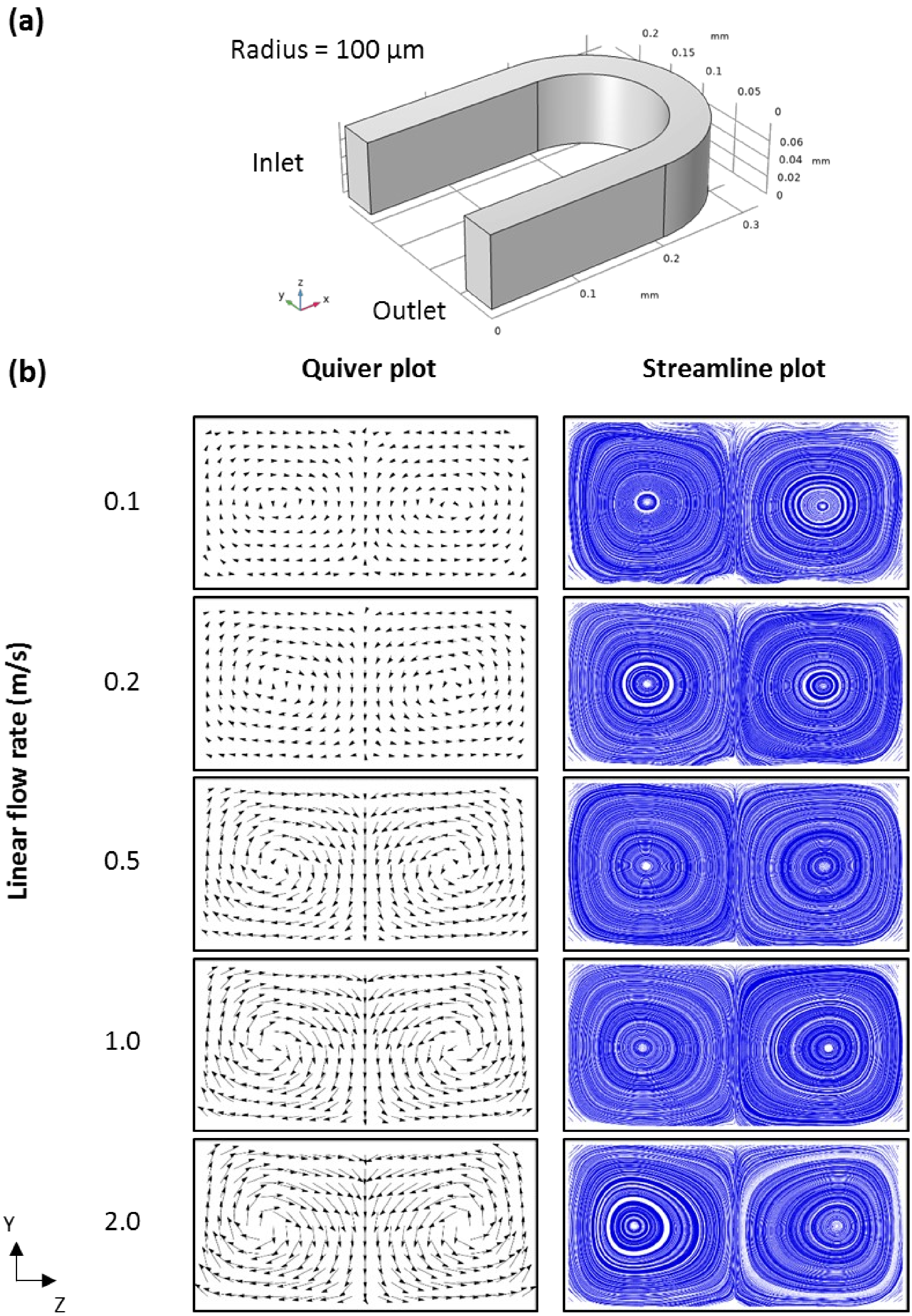

Figure S3. Simulation result of secondary flows induced by a HAR half arc. (a) CFD Model. (b) Quiver and streamline plots of the secondary flow.

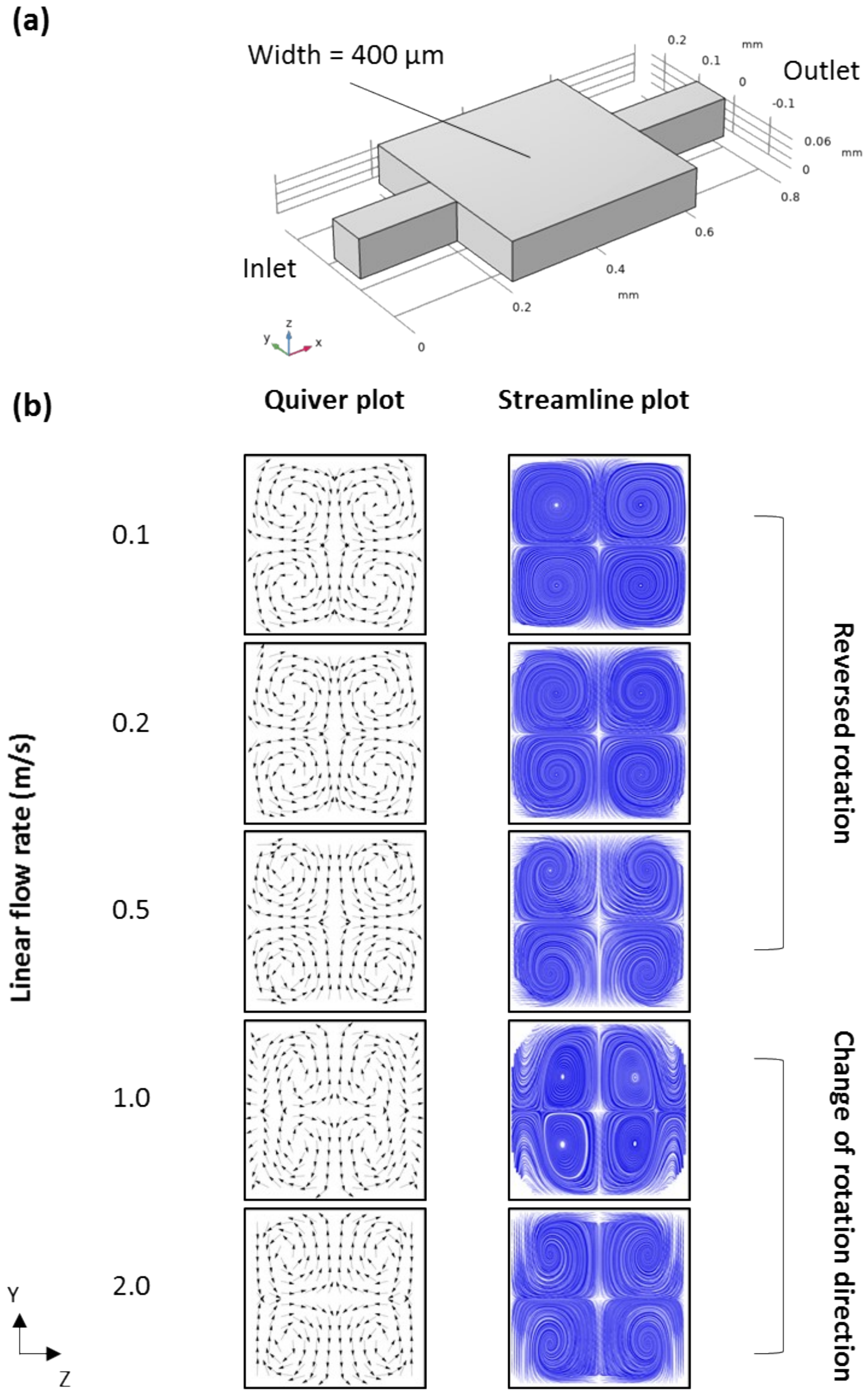

Figure S4. Simulation result of secondary flows induced by a LAR symetric orifice. (a) CFD Model. (b) Quiver and streamline plots of the secondary flow.

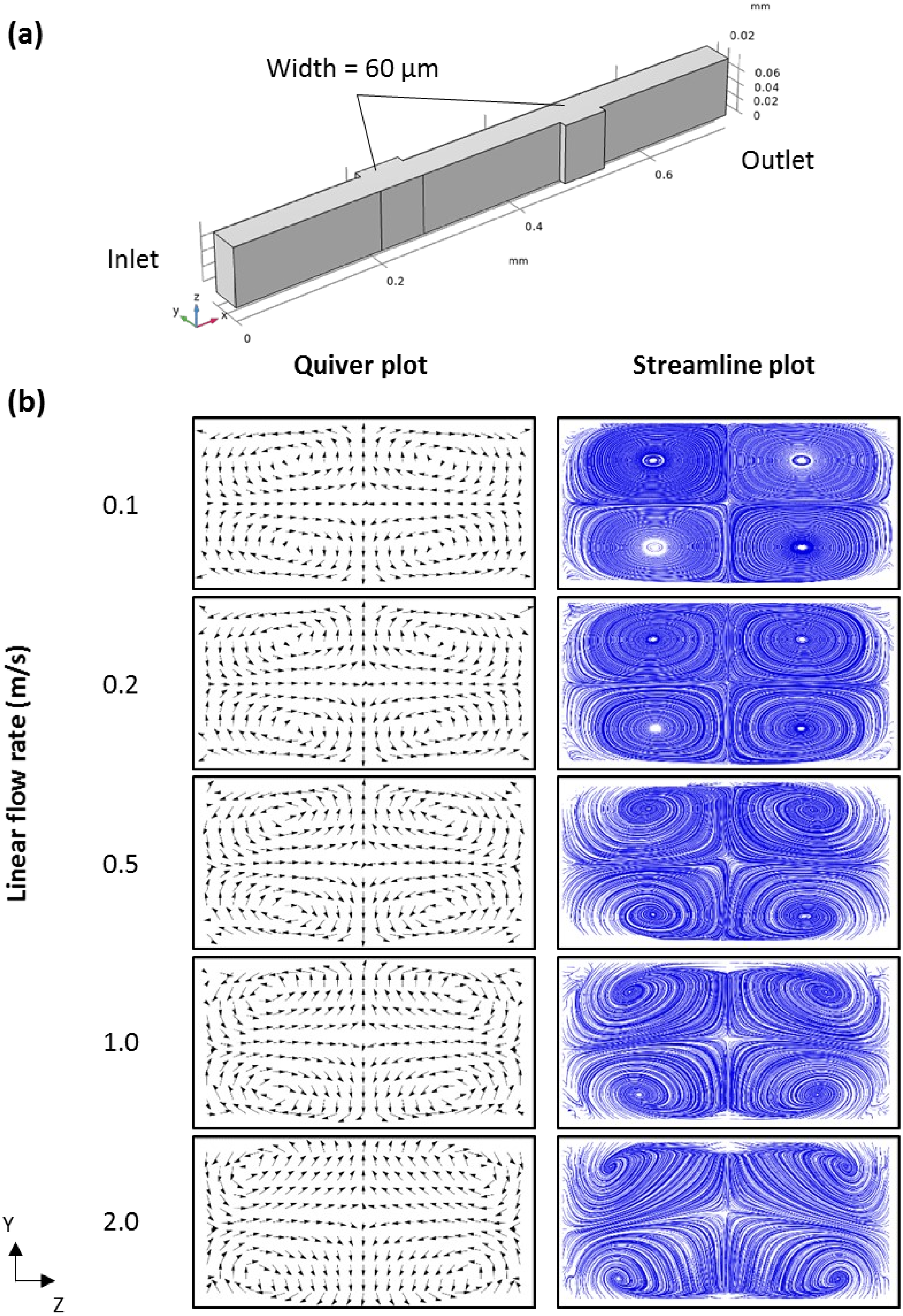

Figure S5. Simulation result of secondary flows induced by an HAR alternating orifice. (a) CFD Model. (b) Quiver and streamline plots of the secondary flow.

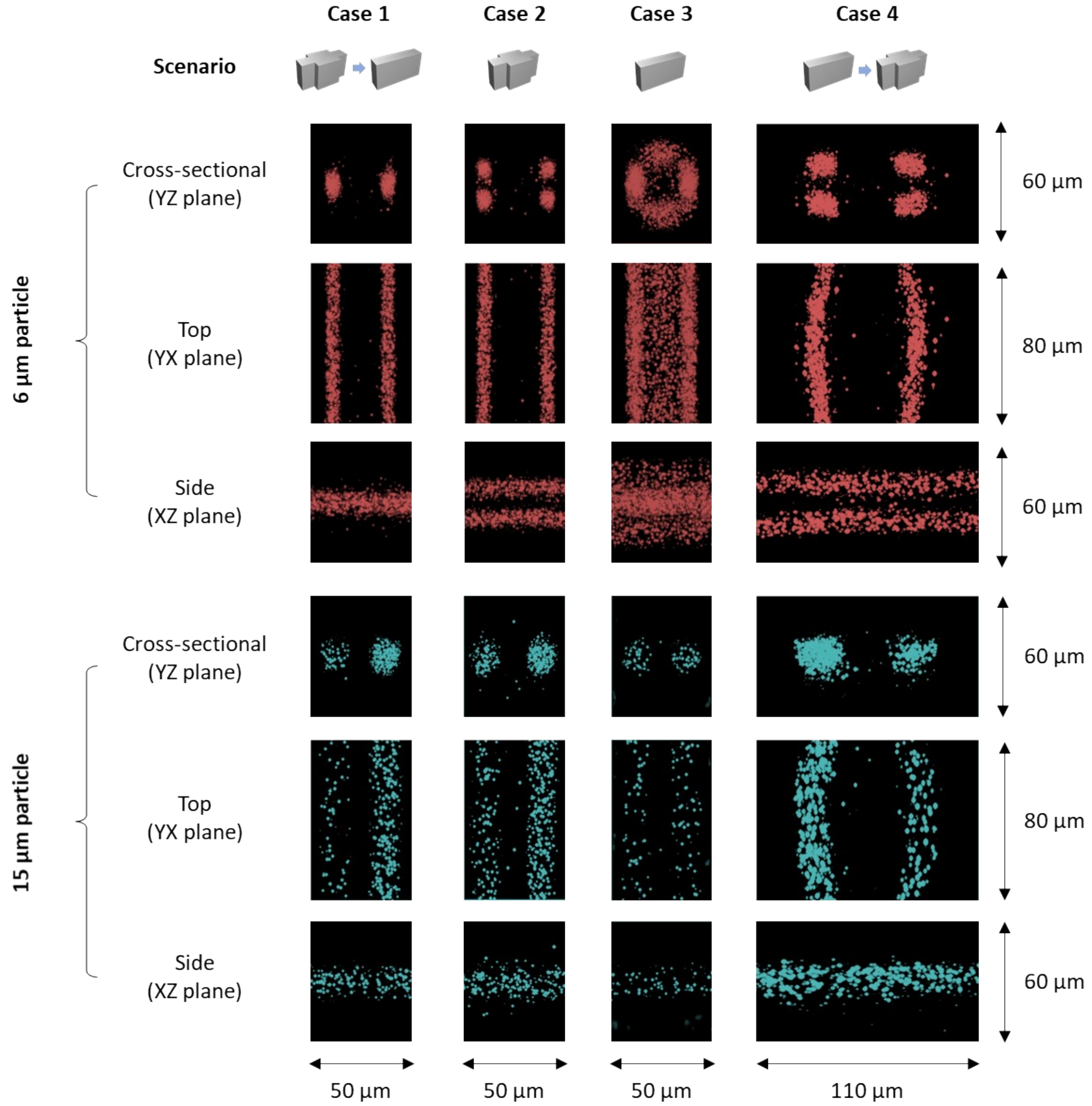

Figure S6. Projected view of particle flow trajectories aquired using a confocal microscope. Top: 6 µm particle; Bottom: 15 µm particle.

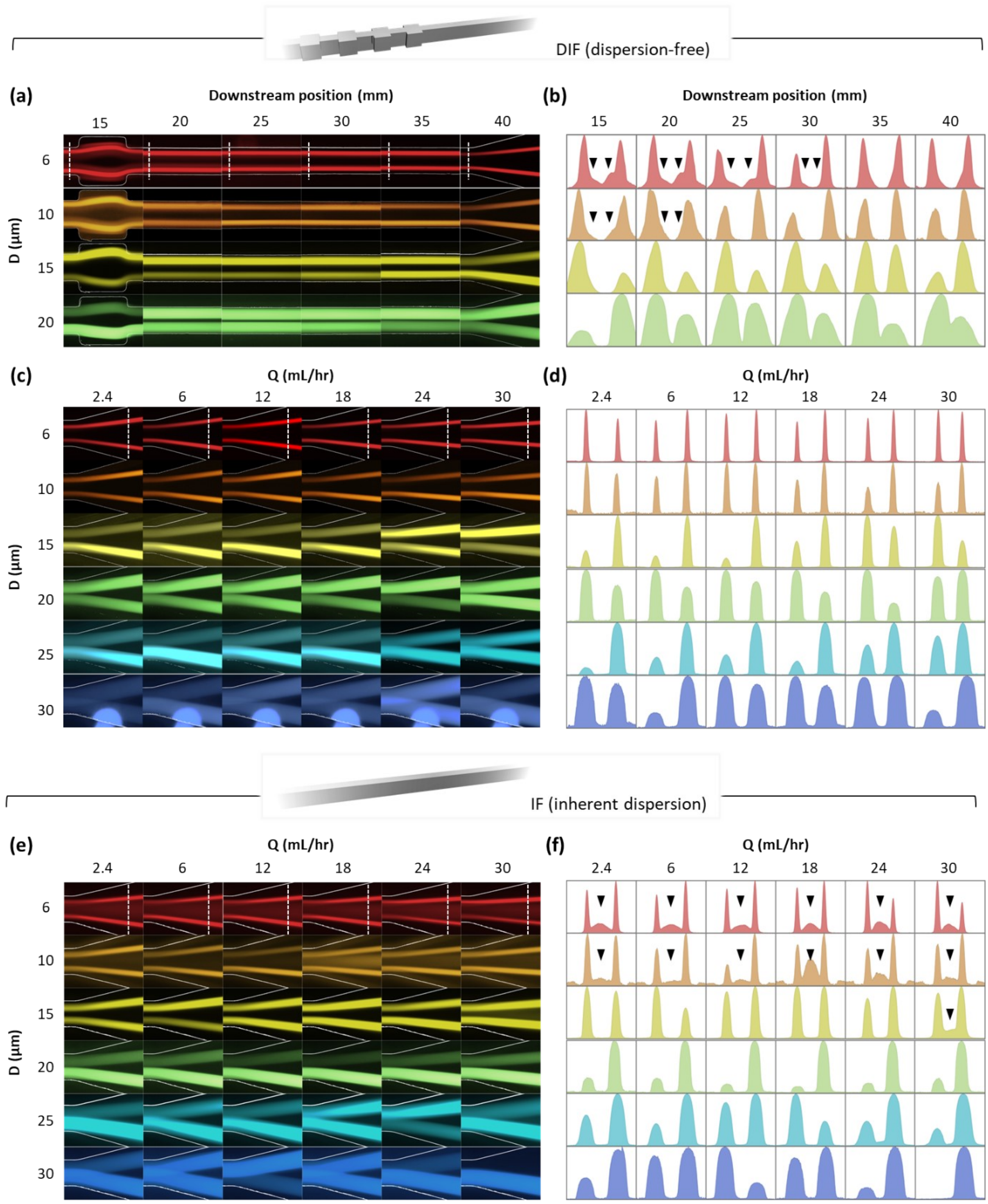

Figure S7. Dispersion of single-plane focusing by DIF (Top) and standard IF (Bottom). Trajectories of 6 different sets of fast-flowing fluorescnece microspheres, each with different size, were individually captured by fluorescence microscopy. **(a-b) Focusing mechanism of DIF**. Imges were captured at 6 downstream positions at the flow rate of 18 mL/hr to visualize the evolution of focusing parttern in DIF system. The intensity profiles at the locations indicated by white dotted lines in (a) are plotted in (b). **(c-f) Consistancy across particle sizes.** Images were captured at different volumetric flow rates (Q) at the downstream distance of 40 mm in (c) DIF system and (e) HAR rectangular straight channel. The intensity profiles at the locations indicated by white dotted lines in (c) and (e) are plottled in (d) and (f), respetively. Scale bar: (a, c, e) 20 μm. (b, d, f) 5 μm.

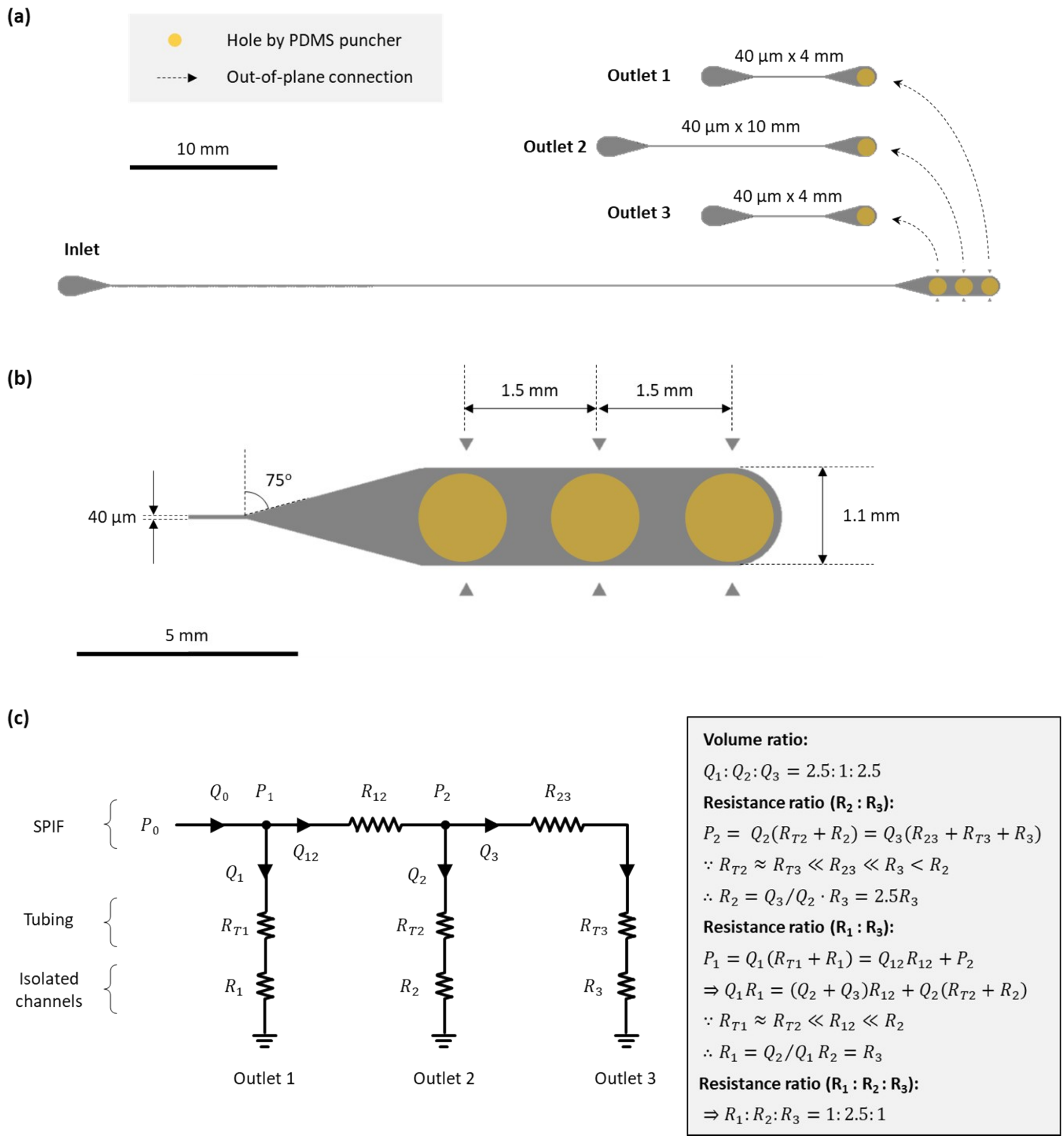

Figure S8. Design of the LIF filter. This filter is designd to delplete 1/6 of input fluid in the middle of the channel cross-section, which corresponds to ~8.9 µm thick layer according to the parabolic flow profile. **(a)** Overview of the LIF filter. **(b)** Zoom-in view of the end of LIF module. **(c)** Equivalent electrical circuit model.

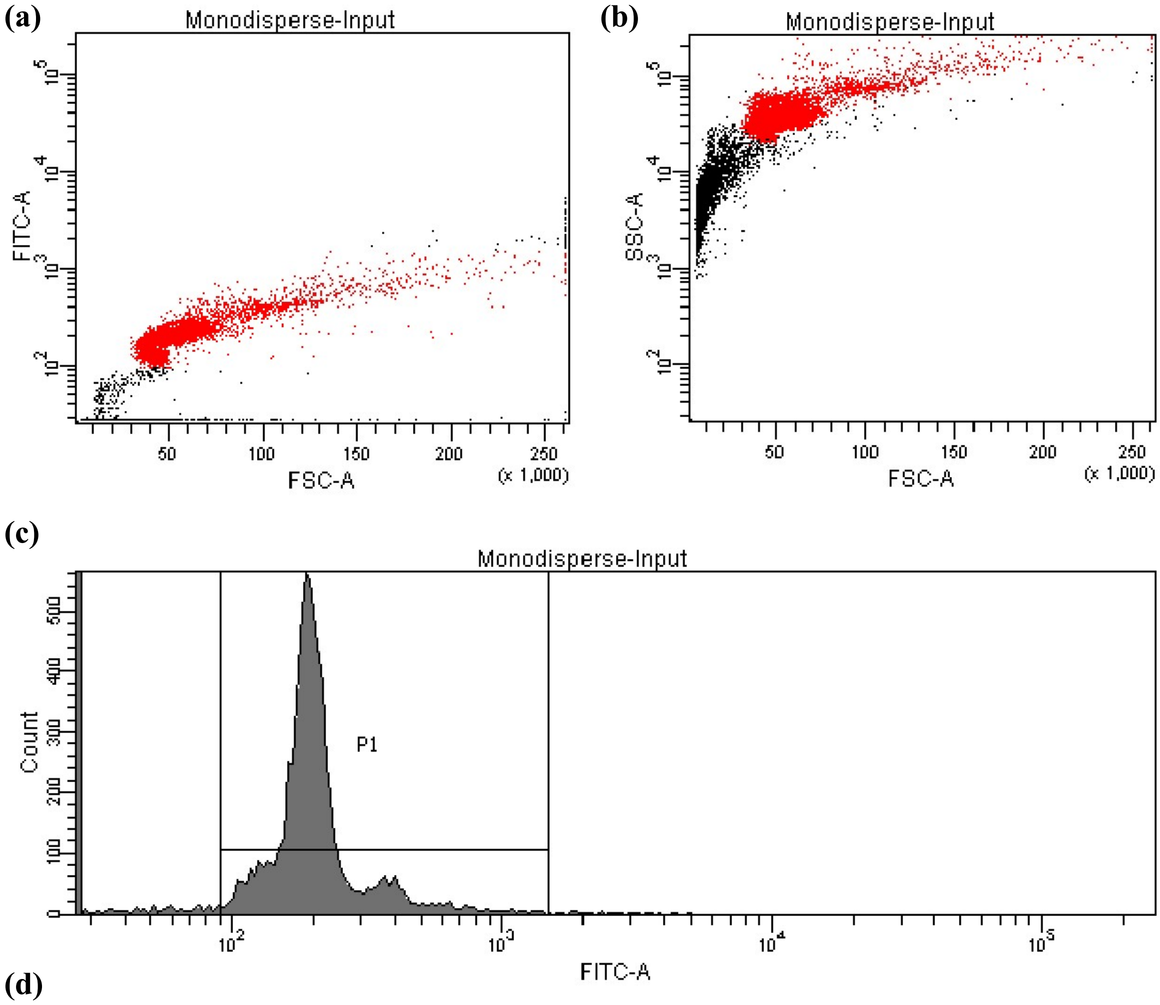

(d)

Experiment Name:	20221114_Kelvin_Filtration_mono
Specimen Name:	Monodisperse
Tube Name:	Input
Record Date:	Nov 14, 2022 3:06:09 PM
$OP:	EEETsia
GUID:	0848118c-7e5d-479d-beba-fd5d787a1b54

Population	#Events	%Parent	FITC-A Mean
All Events	10,000	####	160
P1	6,460	64.6	229

Figure S9. Flow cytometry result of monodisperse sample from the input port. (a) Scatter plot of forward scattering signal (FCS) vs. green fluorescence signal (FITC-A). **(b)** Scatter plot of forward scattering signal (FCS) vs. side scattering signal (SSC-A). **(c)** Histogram of green fluorescence signal (FITC-A). **(d)** Statistics of gating result.

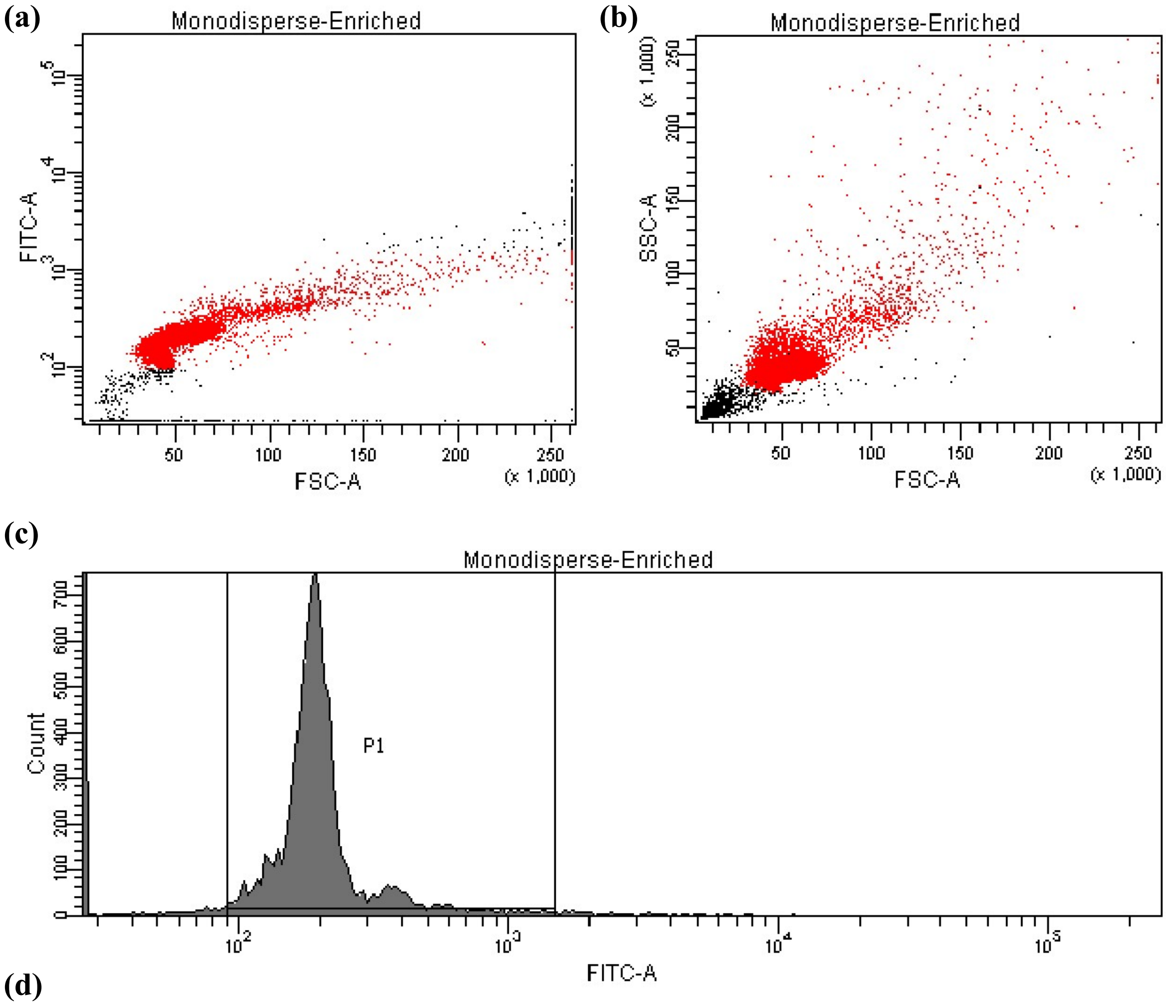

(d)

Experiment Name: 20221114_Kelvin_Filtration_mono
Specimen Name: Monodisperse
Tube Name: Enriched
Record Date: Nov 14, 2022 3:11:56 PM
$OP: EEETsia
GUID: b7ef22d9-5eed-48d9-8516-9bda91c5a55f

Population	#Events	%Parent	FITC-A Mean
All Events	10,000	####	226
P1	8,511	85.1	225

Figure S10. Flow cytometry result of monodisperse sample from the enrichment port. (a) Scatter plot of forward scattering signal (FCS) vs. green fluorescence signal (FITC-A). **(b)** Scatter plot of forward scattering signal (FCS) vs. side scattering signal (SSC-A). **(c)** Histogram of green fluorescence signal (FITC-A). **(d)** Statistics of gating result.

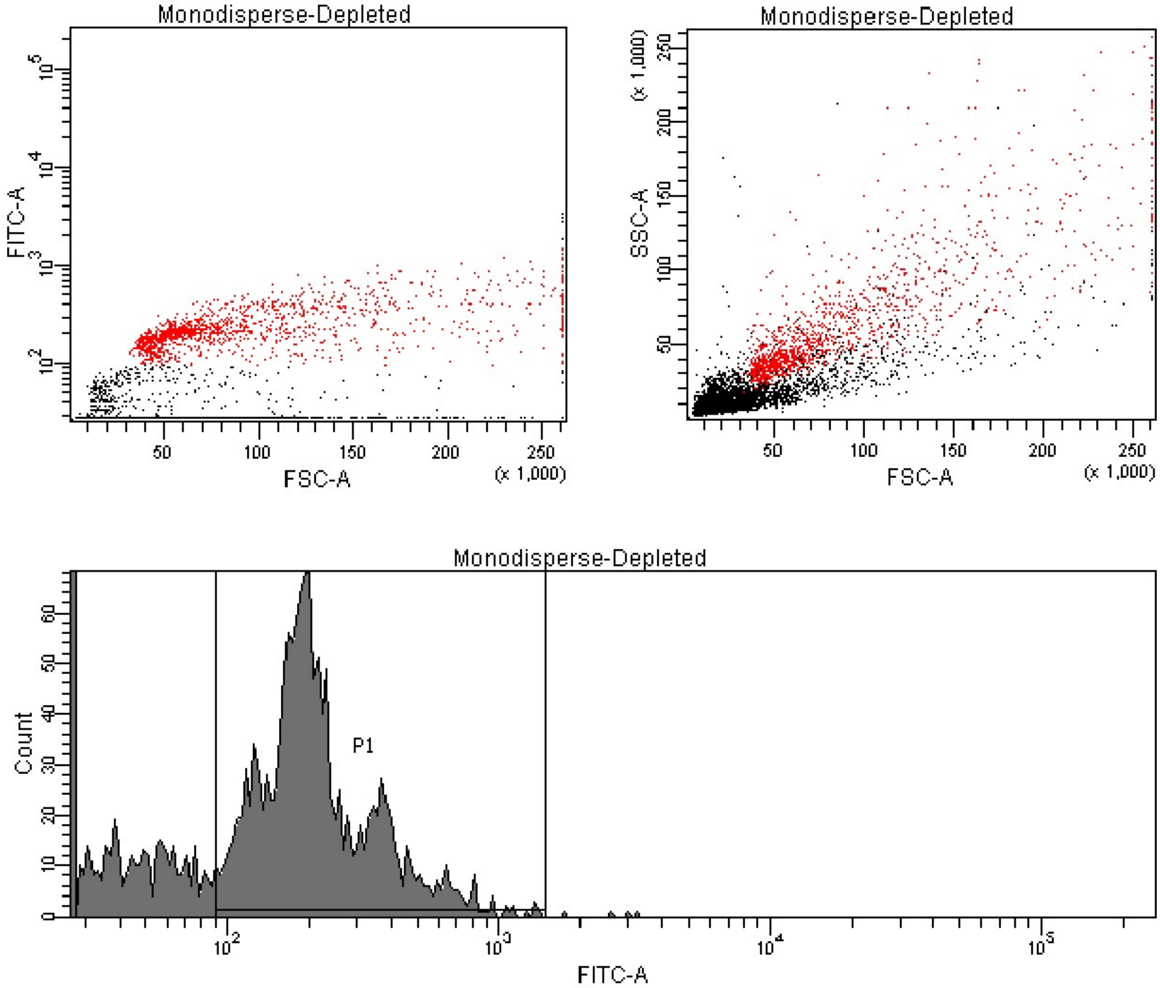

Experiment Name: 20221114_Kelvin_Filtration_mono
Specimen Name: Monodisperse
Tube Name: Depleted
Record Date: Nov 14, 2022 3:18:21 PM
$OP: EEETsia
GUID: e6b0350f-f649-40b3-b68b-865ca19ded06

Population	#Events	%Parent	FITC-A Mean
All Events	10,000	####	38
P1	1,392	13.9	252

Figure S11. Flow cytometry result of monodisperse sample from the depletion port. (a) Scatter plot of forward scattering signal (FCS) vs. green fluorescence signal (FITC-A). **(b)** Scatter plot of forward scattering signal (FCS) vs. side scattering signal (SSC-A). **(c)** Histogram of green fluorescence signal (FITC-A). **(d)** Statistics of gating result.

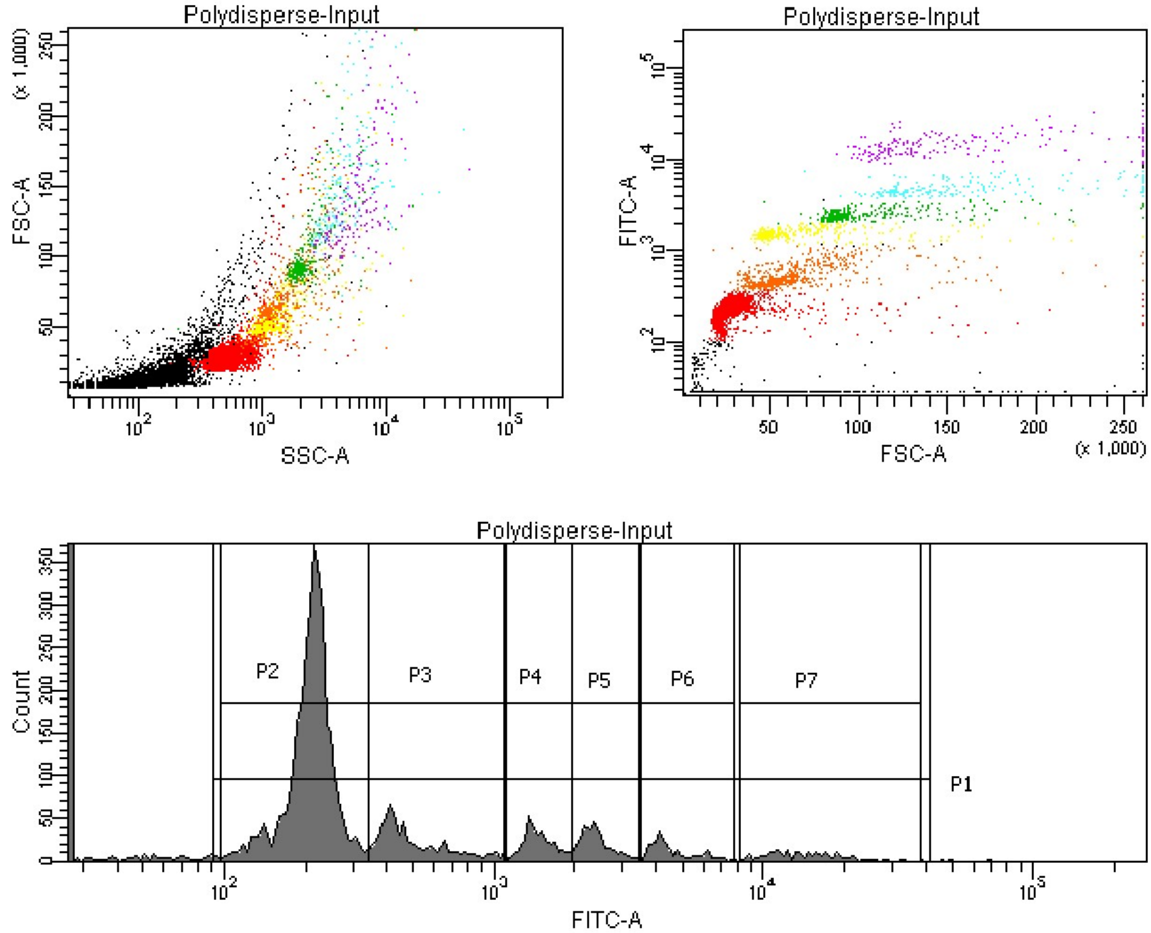

Experiment Name: 20221114_Kelvin_Filtration_poly
Specimen Name: Polydisperse
Tube Name: Input
Record Date: Nov 14, 2022 4:07:35 PM
$OP: EEETsia
GUID: da662533-6745-415b-bcfa-c0adbe5b9864

Population	#Events	%Parent	FITC-A Mean
All Events	10,000	####	623
P2	3,088	30.9	213
P3	625	6.2	525
P4	323	3.2	1,482
P5	315	3.2	2,425
P6	209	2.1	4,681
P7	188	1.9	14,849
P1	4,766	47.7	1,273

Figure S12. Flow cytometry result of polydisperse sample from the input port. (a) Scatter plot of forward scattering signal (FCS) vs. green fluorescence signal (FITC-A). **(b)** Scatter plot of forward scattering signal (FCS) vs. side scattering signal (SSC-A). **(c)** Histogram of green fluorescence signal (FITC-A). **(d)** Statistics of gating result.

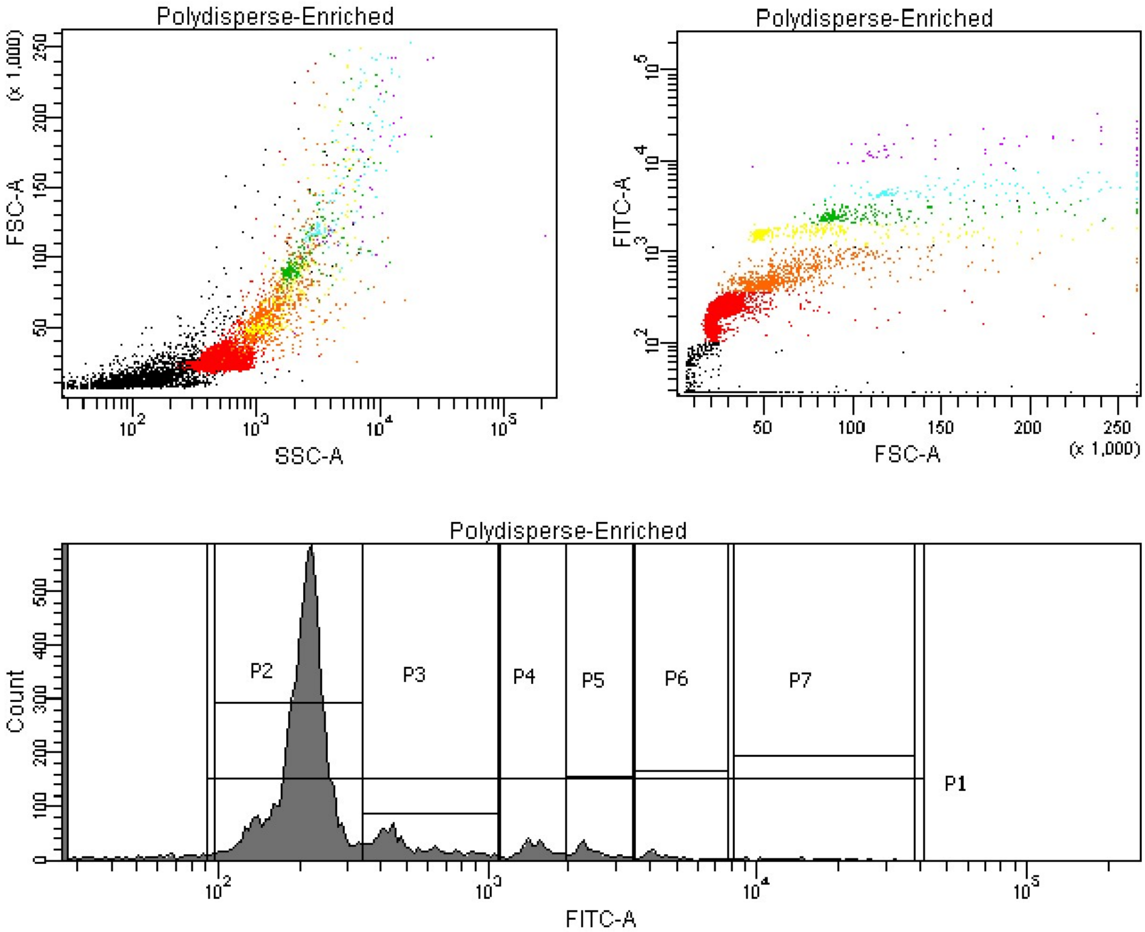

Experiment Name: 20221114_Kelvin_Filtration_poly
Specimen Name: Polydisperse
Tube Name: Enriched
Record Date: Nov 14, 2022 4:16:52 PM
$OP: EEETsia
GUID: 22d2a40b-2d5b-4539-a0ee-e7b25cfd5dcd

Population	#Events	%Parent	FITC-A Mean
All Events	10,000	####	391
P2	5,583	55.8	210
P3	784	7.8	543
P4	276	2.8	1,533
P5	213	2.1	2,453
P6	117	1.2	4,639
P7	53	0.5	14,671
P1	7,052	70.5	554

Figure S13. Flow cytometry result of polydisperse sample from the enrichment port. (a) Scatter plot of forward scattering signal (FCS) vs. green fluorescence signal (FITC-A). **(b)** Scatter plot of forward scattering signal (FCS) vs. side scattering signal (SSC-A). **(c)** Histogram of green fluorescence signal (FITC-A). **(d)** Statistics of gating result.

Supplementary information

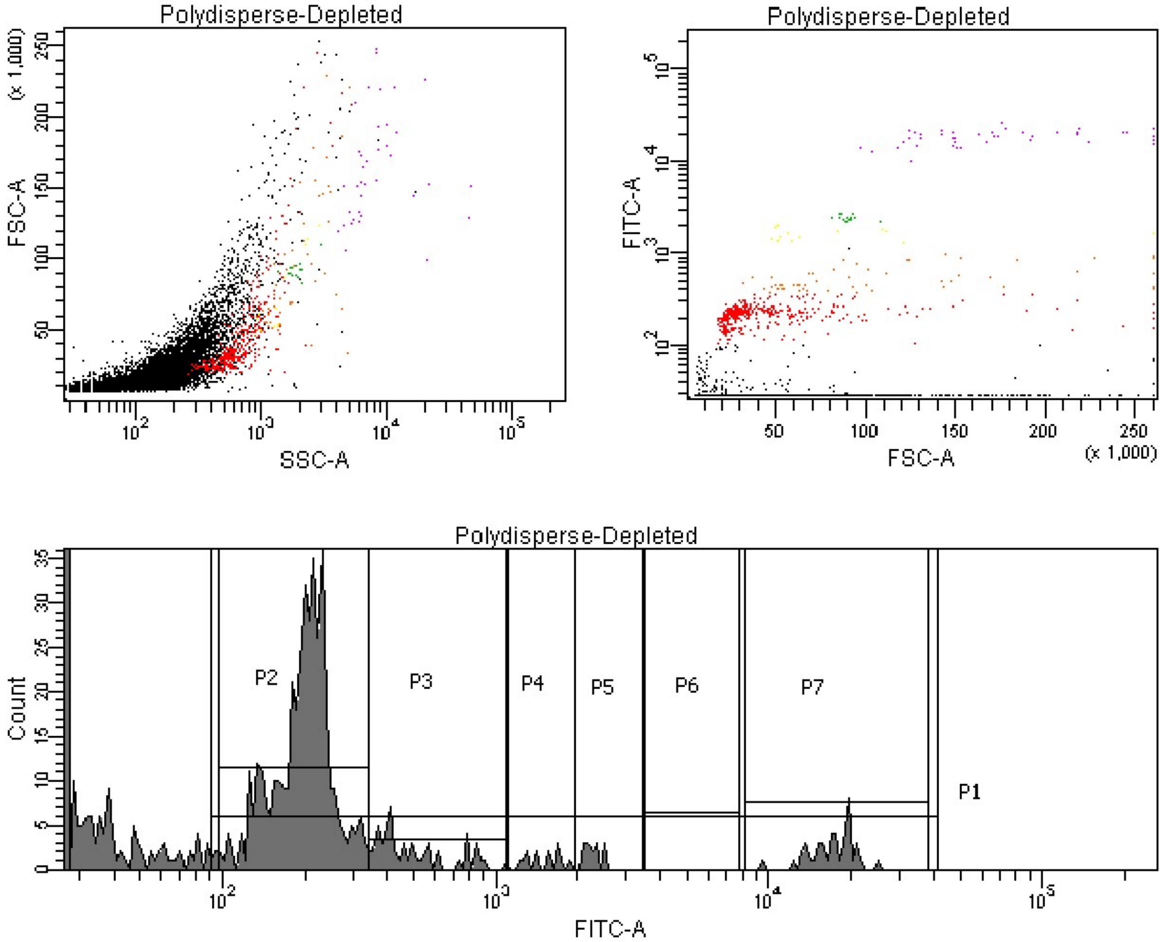

Experiment Name: 20221114_Kelvin_Filtration_poly
Specimen Name: Polydisperse
Tube Name: Depleted
Record Date: Nov 14, 2022 4:29:51 PM
$OP: EEETsia
GUID: ce444559-8206-4792-849a-733b952ab27c

Population	#Events	%Parent	FITC-A Mean
All Events	10,000	####	89
P2	393	3.9	203
P3	53	0.5	518
P4	13	0.1	1,530
P5	14	0.1	2,292
P6	0	0.0	####
P7	42	0.4	17,546
P1	519	5.2	1,729

Figure S14. Flow cytometry result of polydisperse sample from the depletion port. (a) Scatter plot of forward scattering signal (FCS) vs. green fluorescence signal (FITC-A). **(b)** Scatter plot of forward scattering signal (FCS) vs. side scattering signal (SSC-A). **(c)** Histogram of green fluorescence signal (FITC-A). **(d)** Statistics of gating result.

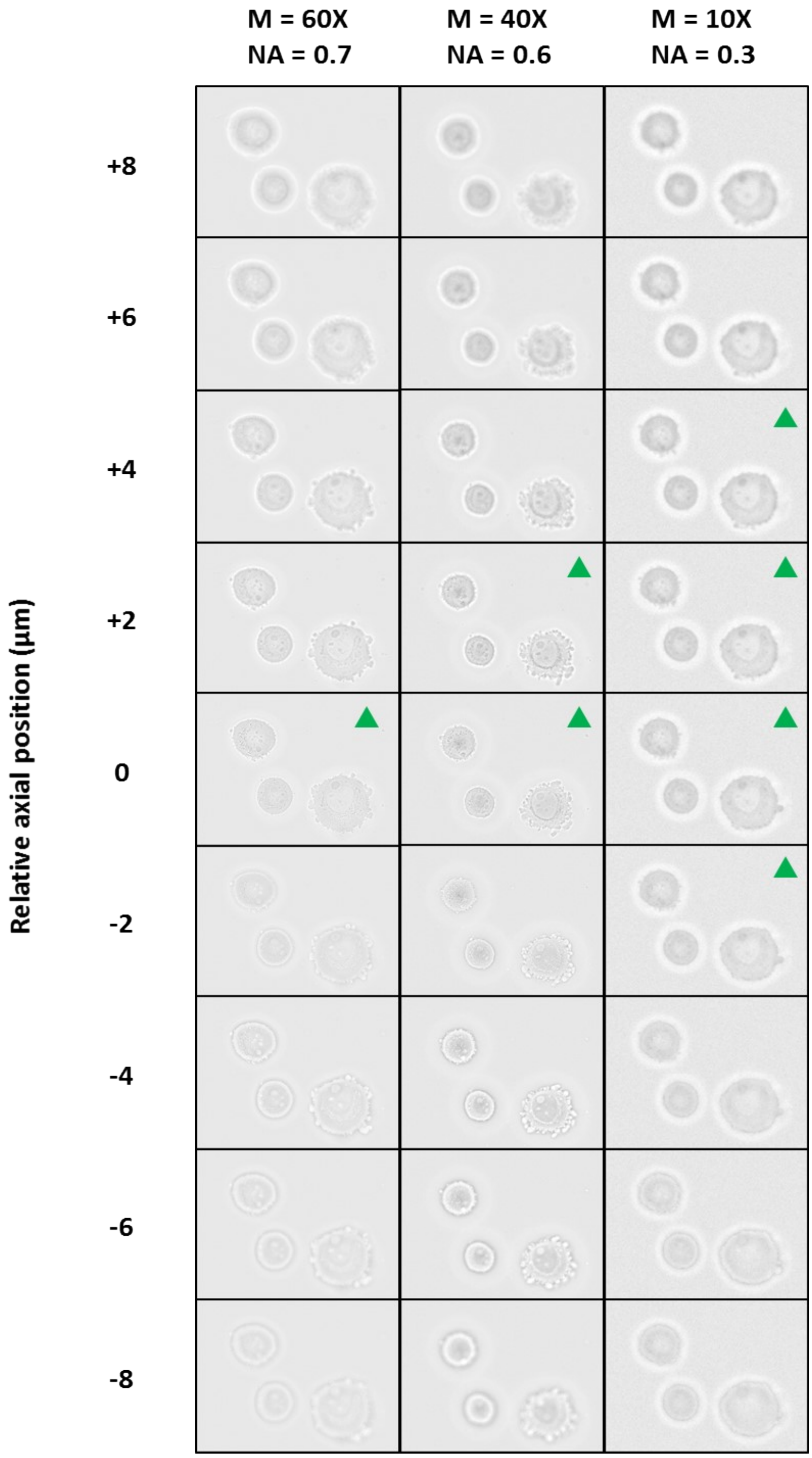

Figure S15. Effect of varying axial (z-) position and numerical aperture (NA) on images. Three MB231 cells were captured at different axial (z-) positions under three different magnifications (M) and numerical aperture (NA). The Rayleigh range are 1.27 µm, 1.73 µm and 6.91 µm for 60X, 40X and 10X magnifications, respectively. Green triangles indicates images in focus.

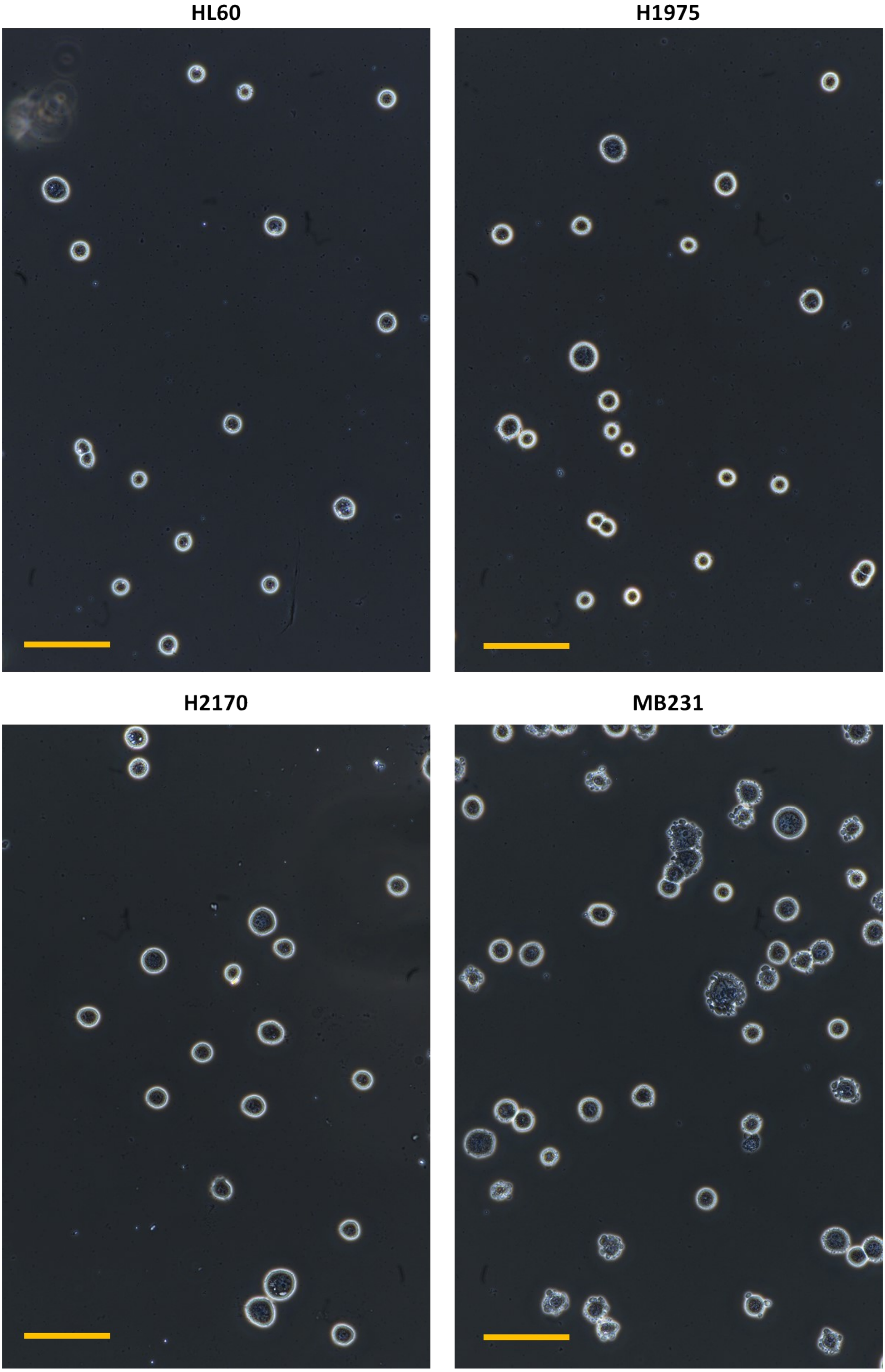

Figure S16. 20X phase-contrasted microscopic images of four cancer cell lines. Scale bar = 100 µm.

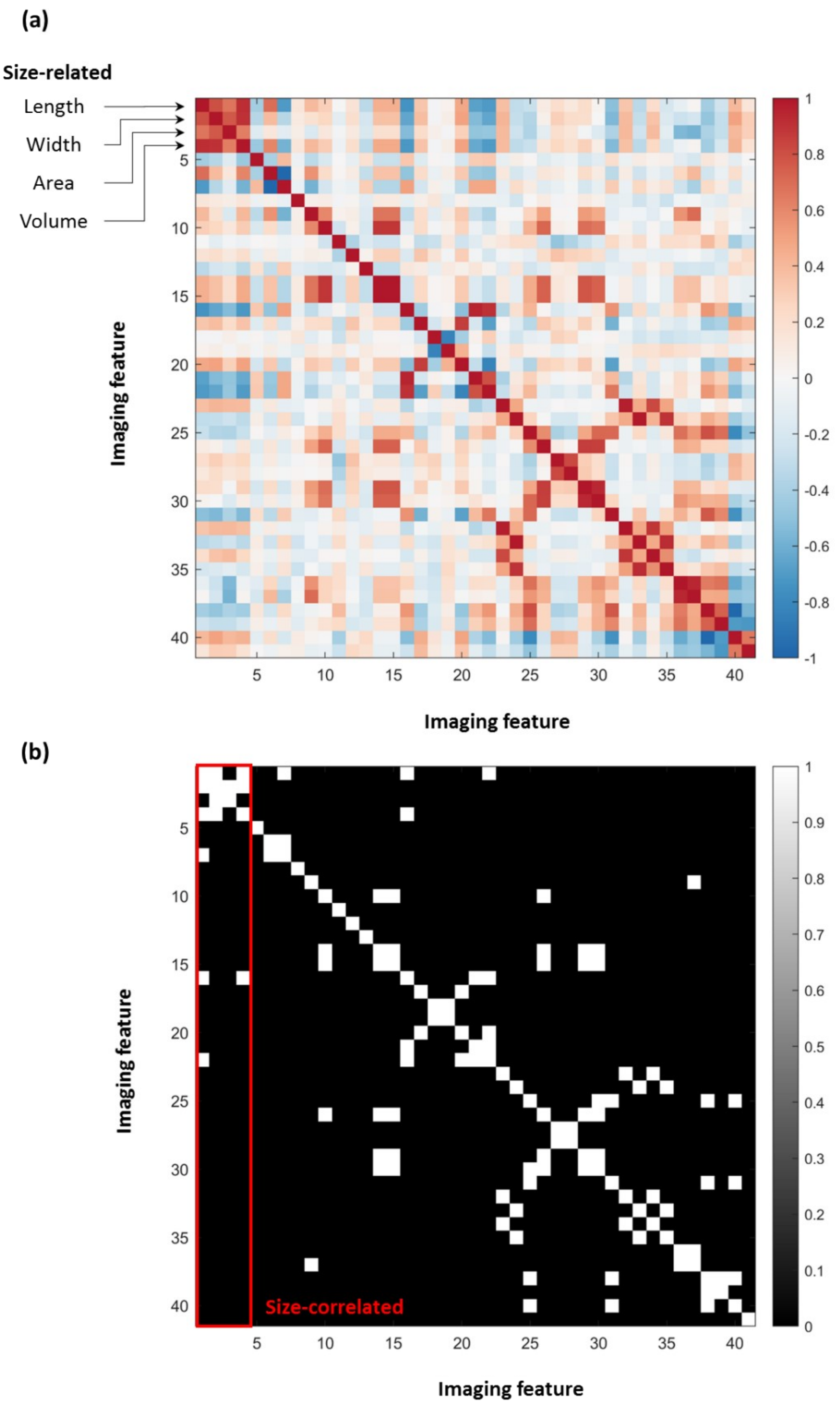

Figure S17. Correlation analysis of 41 imaging features. These features are extracted from the bright-field image and the corresponding binary mask. Details of features refer to Table S1-2. The first four features (i.e., length, width, area and volume) directly relate to particle size. **(a)** Correlation matrix **(b)** Binary matrix showing correlations that have magnitude >0.7. The red box encircles the region referring to size-correlated.

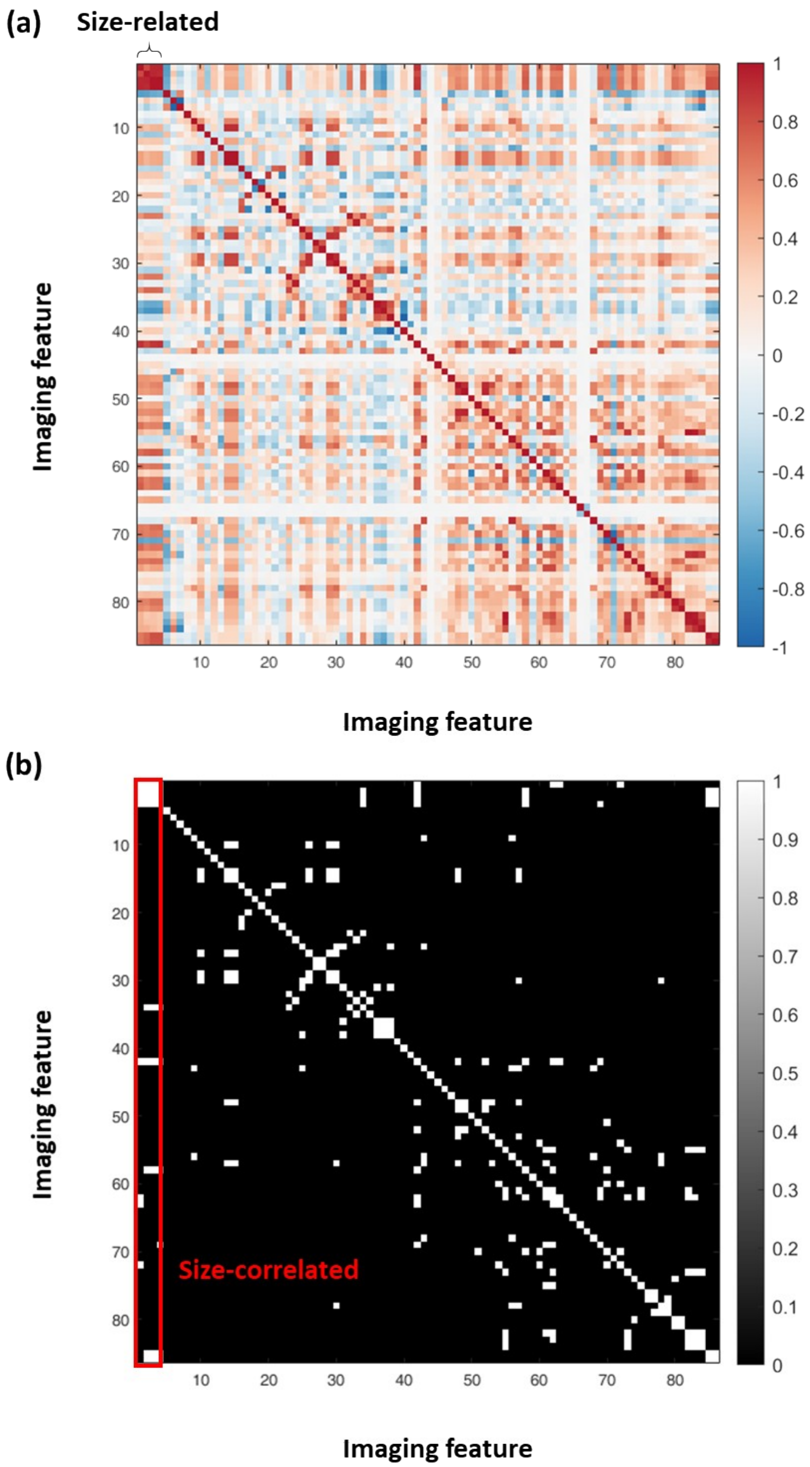

Figure S18. Correlation analysis of 86 imaging features. These features are extracted from the bright-field and quantitative phase images and the corresponding binary mask. Details of features refer to Table S1-2. The first four features (i.e. length, width, area and volume) directly relate to particle size. **(a)** Correlation matrix **(b)** Binary matrix showing correlations that have magnitude >0.7. The red box encircles the region referring to size-correlated.

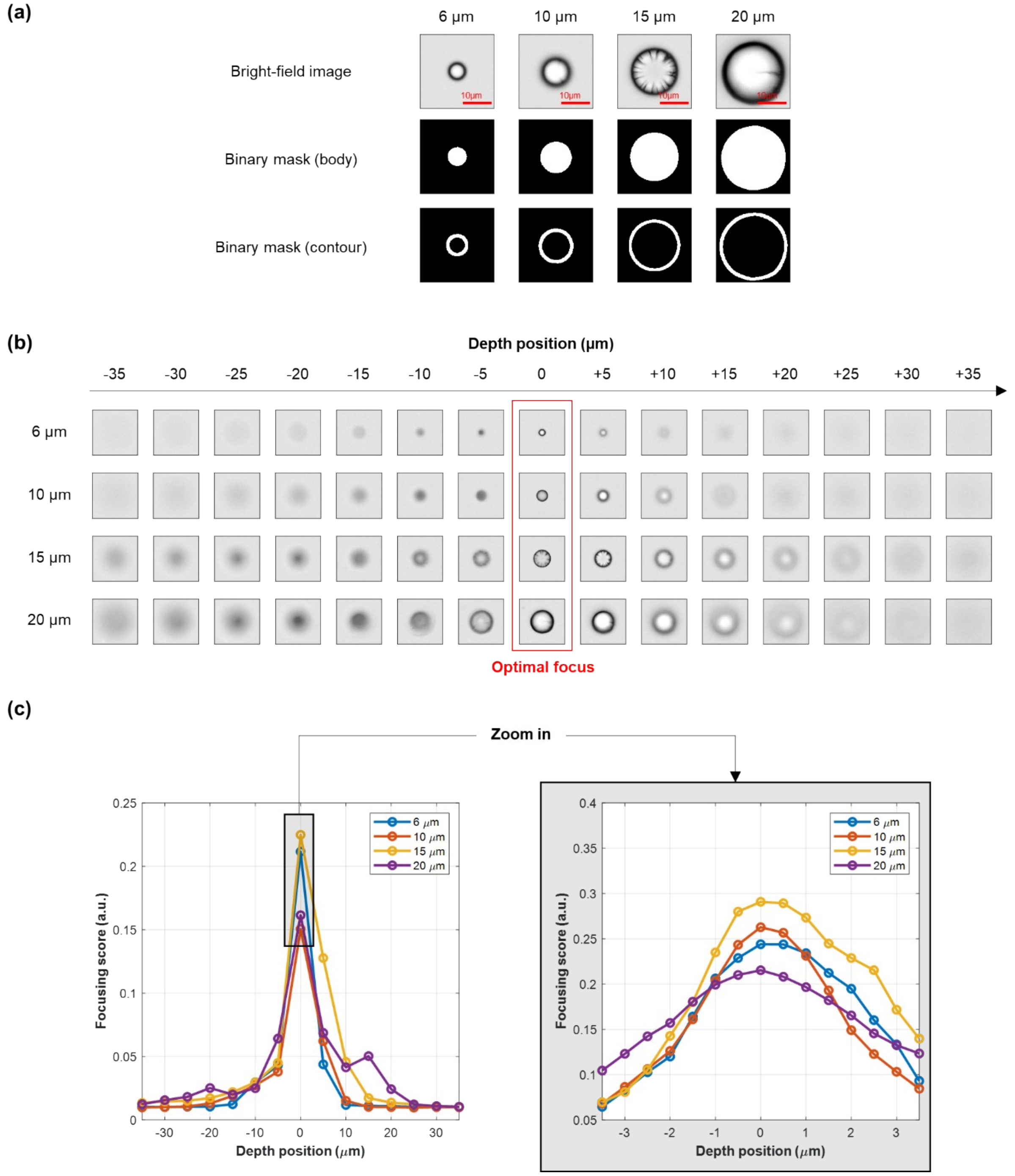

Figure S19. Method to classify focusing condition of microparticles. (a) Bright-field image, the binary mask of body, and the binary mark of contour of 6µm, 10µm, 15 µm, and 20µm microparticles. **(b)** The morphology of particles of different sizes at different depth positions. **(c)** Two line plots showing the focusing score of particles of different sizes at different depth positions. Left: from 35µm to +35µm. Right: from -3µm to +3µm.

Table S1: Ratio of residual zone (equivalently loss) of the HAR rectangular pipe at various particle sizes and flow rates (by direct numerical simulation).

Particle size (μm)	Volumetric flow rate (mL/hr)		
	6	18	30
5	36.7%	38.0%	34.3%
15	13.8%	6.5%	4.8%
20	2.5%	0.0%	0.0%
25	0.0%	0.0%	0.0%

Table S2: Loss of the single-plane DIF system (100%-yield) at various particle sizes and flow rates (by experiment).

Particle size (μm)	Volumetric flow rate (mL/hr)					
	2.4	6	12	18	24	30
6	4.4%	4.2%	3.3%	4.3%	6.1%	5.3%
10	0.2%	0.1%	0.0%	0.0%	0.5%	0.4%
15	0.2%	0.3%	0.1%	0.4%	0.1%	0.2%
20	0.4%	0.5%	0.5%	0.2%	0.0%	0.0%
25	3%	2%	5%	0%	2%	0%

Table S3: Loss of the HAR rectangular pipe (100%-yield) at various particle sizes and flow rates (by experiment).

Particle size (μm)	Volumetric flow rate (mL/hr)					
	2.4	6	12	18	24	30
6	39.9%	33.9%	29.0%	32.2%	34.4%	41.7%
10	15.8%	6.3%	17.5%	22.2%	25.3%	15.6%
15	0.9%	1.7%	1.3%	1.2%	10.2%	16.6%
20	0.8%	0.1%	0.4%	1.0%	0.0%	0.0%
25	2%	4%	2%	2%	1%	0%

Table S4: Area under curve (AUC) of the receiver-operating-characteristic (ROC) curve analysis between 5 types of cells.

		Size correlated	Size uncorrelated	All
Cancer vs. PBMCs classification	PBMC vs. HL60	0.997	0.998	1.000
	PBMC vs. H1975	0.999	0.999	0.999
	PBMC vs. H2170	0.998	0.998	1.000
	PBMC vs. MB231	0.998	1.000	1.000
Cancer type classification	HL60 vs. H1975	0.918	0.936	0.925
	HL60 vs. H2170	0.903	0.937	0.944
	HL60 vs. MB231	0.940	0.988	0.990
	MB231 vs. H1975	0.670	0.896	0.780
	MB231 vs. H2170	0.738	0.935	0.943
Cancer sub-type classification	H1975 vs H2170	0.658	0.796	0.871

Table S5: Equations and variable to characterise dispersion

Description	Variables	Equation/Remarks
Fluorescent intensity	$I(x, q, a)$	$Regarded\ as\ the\ wieghting\ of\ lateral\ position$
Lateral position	x	$Regardd\ as\ the\ dependent\ variable$
Particle diameter	a	
Volumatric flow rate	q	
Number of sample points of particle diameter	n_a	
Number of sample points of volumetric flow rate	n_q	
Total fluorecenct inetnsity	$I_{total}(q, a)$	$\sum_x I(x,q,a)$
Mean lateral position	$\underline{x}(q,a)$	$\sum_x (x \cdot I(x,q,a)) / I_{total}(q,a)$
Standard deviation of lateral position	$\sigma_x(q,a)$	$\sqrt{\sum_x \left(I(x,q,a) \cdot (x - \underline{x}(q,a))^2\right) / I_{total}(q,a)}$
Mean of mean lateral position	$\underline{x}(q)$	$\sum_a (\underline{x}(q,a)) / n_a$
Standard deviation of mean lateral position	$\sigma_{\underline{x}}(q)$	$\sqrt{\sum_a (\underline{x}(q,a) - \underline{x}(q))^2 / n_a}$
Spreading	SP	$\sum_q \sum_a \sigma_x(q,a) / (n_q \cdot n_a)$
Drifting	DR	$\sum_q \sigma_{\underline{x}}(q) / n_q$
Dispersion	$DISP$	$DR + SP$

Table S6: Equations of single-cell features (List of variables used can be found in Table S2)

Feature name	No.	Abbreviation	Equation
Length	1		L_{major}
Width	2		L_{minor}
Area	3	A	$L_{pix}{}^{2} \cdot N_{pix}$
Volume	4	V	$\frac{4}{3}\pi \cdot (\frac{L_{minor}}{2})^{2} \cdot (\frac{L_{major}}{2})$
Circularity	5		$4\pi A/P$
Eccentricity	6		L_{ellip}/L_{major}
Aspect Ratio	7		L_{minor}/L_{major}
Orientation	8		θ_{major}
Attenuation Density	9		$\iint_{A} (1 - OD(x,y))\, dxdy/N_{pix}$
Amplitude Variance	10	$\sigma_{OD}{}^{2}$	$\iint_{A} (OD(x,y) - \underline{OD})^{2}\, dxdy/(N_{pix} - 1)$
Amplitude Skewness	11		$\iint_{A} (OD(x,y) - \underline{OD})^{3}\, dxdy/(N_{pix} \cdot \sigma_{OD}{}^{3})$
Amplitude Kurtosis	12		$\iint_{A} (OD(x,y) - \underline{OD})^{4}\, dxdy/(N_{pix} \cdot \sigma_{OD}{}^{4})$
Peak Amplitude	13		$max\{OD(x,y)\}$
Peak Absorption	14		$min\{OD(x,y)\}$
Amplitude Range	15		$\{OD(x,y)\} - min\{OD(x,y)\}$
BF Entropy Mean	16	$\underline{OD_{ent}}$	$\frac{\iint_{A} OD_{ent}(x,y)\, dxdy}{N_{pix}}$
BF Entropy Variance	17	$\sigma_{ODent}{}^{2}$	$\iint_{A} (OD_{ent}(x,y) - \underline{OD_{ent}})^{2} dxdy/(N_{pix} - 1)$
BF Entropy Skewness	18		$\iint_{A} (OD_{ent}(x,y) - \underline{OD_{ent}})^{3} dxdy/(N_{pix} \cdot \sigma_{ODent}{}^{3})$
BF Entropy Kurtosis	19		$\iint_{A} (OD_{ent}(x,y) - \underline{OD_{ent}})^{4} dxdy/(N_{pix} \cdot \sigma_{ODent}{}^{4})$

BF Entropy Range	20		$\{OD_{ent}(x,y)\} - min\{OD_{ent}(x,y)\}$
BF Entropy Peak	21		$max\{OD_{ent}(x,y)\}$
BF Entropy Min	22		$min\{OD_{ent}(x,y)\}$
BF Entropy Centroid Displacement	23		$\sqrt{(x_{ODent,cen} - x_{cen})^2 + (y_{ODent,cen} - y_{cen})^2} \cdot L_{pix}$
BF Entropy Radial Distribution	24		$\frac{\iint_A r \cdot OD_{ent}(r,\theta)\, drd\theta}{\iint_A OD_{ent}(r,\theta)\, drd\theta}$
BF STD Mean	25	$\underline{OD_{STD}}$	$\frac{\iint_A OD_{STD}(x,y)\, dxdy}{N_{pix}}$
BF STD Variance	26	${\sigma_{ODstd}}^2$	$\frac{\iint_A (OD_{STD}(x,y) - \underline{OD_{STD}})^2 dxdy}{N_{pix} - 1}$
BF STD Skewness	27		$\frac{\iint_A (OD_{STD}(x,y) - \underline{OD_{STD}})^3 dxdy/N_{pix}}{{\sigma_{ODstd}}^3}$
BF STD Kurtosis	28		$\frac{\iint_A (OD_{STD}(x,y) - \underline{OD_{STD}})^4 dxdy/N_{pix}}{{\sigma_{ODstd}}^4}$
BF STD Range	29		$\{OD_{STD}(x,y)\} - min\{OD_{STD}(x,y)\}$
BF STD Peak	30		$max\{OD_{STD}(x,y)\}$
BF STD Min	31		$min\{OD_{STD}(x,y)\}$
BF STD Centroid Displacement	32		$\sqrt{(x_{ODSTD,cen} - x_{cen})^2 + (y_{ODSTD,cen} - y_{cen})^2} \cdot L_{pix}$
BF STD Radial Distribution	33		$\frac{\iint_A r \cdot OD_{STD}(r,\theta)\, drd\theta}{\iint_A OD_{STD}(r,\theta)\, drd\theta}$
BF Fiber Texture Centroid Displacement	34		$\sqrt{(x_{ODfiber,cen} - x_{cen})^2 + (y_{ODfiber,cen} - y_{cen})^2} \cdot L_{pix}$
BF Fiber Texture Radial Distribution	35		$\frac{\iint_A r \cdot OD_{fiber}(r,\theta)\, drd\theta}{\iint_A OD_{fiber}(r,\theta)\, drd\theta}$

BF Fiber Texture Pixel>Upper Percentile	36		$\frac{Number\ of\ pixels\ in\ OD_{fiber}(x,y) > 75th\ percentile}{N_{pix}}$
BF Fiber Texture Pixel>Median	37		$\frac{Number\ of\ pixels\ in\ OD_{fiber}(x,y) > median}{N_{pix}}$
BF Fiber Mean	38	$\underline{OD_{fiber}}$	$\frac{\iint_A OD_{fiber}(x,y)\ dxdy}{N_{pix}}$
BF Fiber Variance	39	${\sigma_{ODfiber}}^2$	$\frac{\iint_A (OD_{fiber}(x,y) - \underline{OD_{fiber}})^2\ dxdy}{N_{pix} - 1}$
BF Fiber Skewness	40		$\frac{\iint_A (OD_{fiber}(x,y) - \underline{OD_{fiber}})^3 dxdy/N_{pix}}{{\sigma_{ODfiber}}^3}$
BF Fiber Kurtosis	41		$\frac{\iint_A (OD_{fiber}(x,y) - \underline{OD_{fiber}})^4 dxdy/N_{pix}}{{\sigma_{ODfiber}}^4}$
Dry Mass	42	MD_{total}	$\frac{\lambda}{2\pi\alpha}\iint_A MD(x,y)\ dxdy$
Dry Mass Density	43	$\underline{DMD}$	$\iint_A DMD(x,y)\ dxdy/N_{pix}$
Dry Mass Variance	44	${\sigma_{DMD}}^2$	$\iint_A (DMD(x,y) - \underline{DMD})^2\ dxdy/(N_{pix} - 1)$
Dry Mass Skewness	45		$\iint_A (DMD(x,y) - \underline{DMD})^3\ dxdy/(N_{pix} \cdot {\sigma_{DMD}}^3)$
Dry Mass Radial Distribution	46		$\frac{\iint_A DMD(r,\theta)\ r\ drd\theta}{\iint_A DMD(r,\theta)\ drd\theta}$
Dry Mass Centroid Displacement	47		$\sqrt{(x_{DMD,cen} - x_{cen})^2 + (y_{DMD,cen} - y_{cen})^2} \cdot L_{pix}$
Peak Phase	48		$max\{MD(x,y)\}$
Phase Variance	49	${\sigma_{MD}}^2$	$\iint_A (MD(x,y) - \underline{MD})^2\ dxdy/(N_{pix} - 1)$
Phase Skewness	50		$\iint_A (MD(x,y) - \underline{MD})^3\ dxdy/(N_{pix} \cdot {\sigma_{MD}}^3)$
Phase Kutosis	51		$\iint_A (MD(x,y) - \underline{MD})^4\ dxdy/(N_{pix} \cdot {\sigma_{MD}}^4)$
Phase Range	52		$max\{MD(x,y)\} - min\{MD(x,y)\}$

Phase Minimum	53		$min\{MD(x,y)\}$
Phase Radial Distribution	54		$\frac{\iint_A r \cdot MD(r,\theta)\, drd\theta}{\iint_A MD(r,\theta)\ \ drd\theta}$
Phase Centroid Displacement	55		$\sqrt{(x_{DMD,cen}-x_{cen})^2+(y_{DMD,cen}-y_{cen})^2}\cdot L_{pix}$
Phase STD Mean	56	$\underline{MD_{STD}}$	$\frac{\iint_A MD_{STD}(x,y)\, dxdy}{N_{pix}}$
Phase STD Var	57	${\sigma_{MDstd}}^2$	$\frac{\iint_A (MD_{STD}(x,y)-\underline{MD_{STD}})^2 dxdy}{N_{pix}-1}$
Phase STD Skewness	58		$\frac{\iint_A (MD_{STD}(x,y)-\underline{MD_{STD}})^3 dxdy/N_{pix}}{{\sigma_{MDstd}}^3}$
Phase STD Kurtosis	59		$\frac{\iint_A (MD_{STD}(x,y)-\underline{MD_{STD}})^4 dxdy/N_{pix}}{{\sigma_{MDstd}}^4}$
Phase STD Centroid Displacement	60		$\sqrt{(x_{MDSTD,cen}-x_{cen})^2+(y_{MDSTD,cen}-y_{cen})^2}\cdot L_{pix}$
Phase SRD Radial Distribution	61		$\frac{\iint_A r \cdot MD_{STD}(r,\theta)\, drd\theta}{\iint_A MD_{STD}(r,\theta)\ \ drd\theta}$
Fit Texture Mean	62	$\underline{MD_{fit}}$	$\frac{\iint_A MD_{fit}(x,y)\, dxdy}{N_{pix}}$
Fit Texture Variance	63	${\sigma_{MDfit}}^2$	$\frac{\iint_A (MD_{fit}(x,y)-\underline{MD_{fit}})^2 dxdy}{N_{pix}-1}$
Fit Texture Skewness	64		$\frac{\iint_A (MD_{fit}(x,y)-\underline{MD_{fit}})^3 dxdy/N_{pix}}{{\sigma_{MDfit}}^3}$
Fit Texture Kurtosis	65		$\frac{\iint_A (MD_{fit}(x,y)-\underline{MD_{fit}})^4 dxdy/N_{pix}}{{\sigma_{MDfit}}^4}$
Fit Texture Centroid Displacement	66		$\sqrt{(x_{MDfit,cen}-x_{cen})^2+(y_{MDfit,cen}-y_{cen})^2}\cdot L_{pix}$

Fit Texture Radial Distribution	67		$\frac{\iint_A r \cdot MD_{fit}(r,\theta)\, drd\theta}{\iint_A MD_{fit}(r,\theta)\, drd\theta}$
Phase Entropy Mean	68	$\underline{MD_{ent}}$	$\frac{\iint_A MD_{ent}(x,y)\, dxdy}{N_{pix}}$
Phase Entropy Var	69	$\sigma_{MDent}{}^2$	$\frac{\iint_A (MD_{ent}(x,y) - \underline{MD_{ent}})^2 dxdy}{N_{pix} - 1}$
Phase Entropy Skewness	70		$\frac{\iint_A (MD_{ent}(x,y) - \underline{MD_{ent}})^3 dxdy/N_{pix}}{\sigma_{MDent}{}^3}$
Phase Entropy Kurtosis	71		$\frac{\iint_A (MD_{ent}(x,y) - \underline{MD_{ent}})^4 dxdy/N_{pix}}{\sigma_{MDent}{}^4}$
Phase Entropy Centroid Displacement	72		$\sqrt{(x_{MDent,cen} - x_{cen})^2 + (y_{MDent,cen} - y_{cen})^2} \cdot L_{pix}$
Phase Entropy Radial Distribution	73		$\frac{\iint_A r \cdot MD_{ent}(r,\theta)\, drd\theta}{\iint_A MD_{ent}(r,\theta)\, drd\theta}$
Phase Fiber Centroid Displacement	74		$\sqrt{(x_{MDfiber,cen} - x_{cen})^2 + (y_{MDfiber,cen} - y_{cen})^2} \cdot L_{pix}$
Phase Fiber Radial Distribution	75		$\frac{\iint_A r \cdot MD_{fiber}(r,\theta)\, drd\theta}{\iint_A MD_{fiber}(r,\theta)\, drd\theta}$
Phase Fiber Pixel>Upper Percentile	76		$\frac{Number\ of\ pixels\ in\ MD_{fiber}(x,y) > 75th\ percentile}{N_{pix}}$
Phase Fiber Pixel>Median	77		$\frac{Number\ of\ pixels\ in\ MD_{fiber}(x,y) > median}{N_{pix}}$
Phase Fiber Mean	78	$\underline{MD_{fiber}}$	$\frac{\iint_A MD_{fiber}(x,y)\, dxdy}{N_{pix}}$
Phase Fiber Var	79	$\sigma_{MDfiber}{}^2$	$\frac{\iint_A (MD_{fiber}(x,y) - \underline{MD_{fiber}})^2\, dxdy}{N_{pix} - 1}$
Phase Fiber Skewness	80		$\frac{\iint_A (MD_{fiber}(x,y) - \underline{MD_{fiber}})^3 dxdy/N_{pix}}{\sigma_{MDfiber}{}^3}$

Phase Fiber Kurtosis	81		$\frac{\iint_A (MD_{fiber}(x,y) - \underline{MD_{fiber}})^4 dxdy/N_{pix}}{\sigma_{MDfiber}{}^4}$
Mean Phase Arrangement	82		$\frac{\iint_A MD(r,\theta)\, r\, drd\theta}{\iint_A MD(r,\theta)\ drd\theta}$
Phase Arrangement Variance	83	$\sigma_{MDarr}{}^2$	$\frac{\iint_A (MD(r,\theta)\, r)^2\, drd\theta}{\iint_A MD(r,\theta)\ drd\theta}$
Phase Arrangement Skewness	84		$\frac{\iint_A (MD(r,\theta) \cdot\ r)^3\, drd\theta}{\sigma_{MDarr}{}^2 \cdot \iint_A MD(r,\theta)\ drd\theta}$
Phase Orientation Variance	85	$\sigma_{MDang}{}^2$	$\frac{\int_0^\infty (\tilde{M}D(\omega) \cdot\ \omega)^2\, d\omega}{\int_0^\infty \tilde{M}D(\omega)\, d\omega}$
Phase Orientation Kurtosis	86		$\frac{\int_0^\infty (\tilde{M}D(\omega) \cdot\ \omega)^4\, d\omega}{\sigma_{MDang}{}^2 \cdot \int_0^\infty \tilde{M}D(\omega)\, d\omega}$

Table S7: Variables and abbreviations of single-cell features

Variable	Description	Equation/Remarks
C	Contour of binary mask	
CM	Cell mask function	$CM(x,y) = \{ 1,\ \ 0 \ \ if\ inside\ cell\ otherwise$
DMD	Dry mas density map	$DMD(x,y) = \frac{\lambda \cdot MD(x,y)}{2\pi\alpha \cdot h(x,y)}$
h	Cell height map	$h(x,y) = \sqrt{(\frac{L_{minor} + L_{major}}{2})^2 - ((x - x_{cen})^2 + (y - y_{cen})^2)}$
L_{ellip}	Distance between foci of ellipse	
L_{major}	Major axis length	
L_{minor}	Minor axis length	
L_{pix}	Physical length of one pixel	
□□	Mass density map (QP contrast)	□□(□,□)
$MD(\theta)$	Mass density projected to polar angle	
$\tilde{MD}(\omega)$	Mass density in angular frequency domain	$\tilde{MD}(\omega) = F(MD(\theta))$
MD□□□,□□□(□,□)	Mean value of QPI within STD filter kernel	$\int_{x-\frac{w_{STD}}{2}}^{x+\frac{w_{STD}}{2}} \int_{y-\frac{w_{STD}}{2}}^{y+\frac{w_{STD}}{2}} MD(u,v)\, dvdu \Big/ {w_{STD}}^2$
$MD_{STD}(x,y)$	QPI STD map	$\int_{x-w_{STD}/2}^{x+w_{STD}/2} \int_{y-w_{STD}/2}^{y+w_{STD}/2} \sqrt{\frac{(MD(u,v) - \underline{MD_{STD,ker}}(x,y))^2}{{w_{STD}}^2}}\, dvdu$
$MD_{cubic}(x,y)$	Cubic polynomial surface fit of mass density map	
$MD_{fit}(x,y)$	Fit texture map of mass density map	$MD(x,y) - MD_{cubic}(x,y)$
$MD_{ent}(x,y)$	Entropy filtered mass density map	$\sum_{k=0}^{255} p_{MD,k} \cdot p_{MD,k}$

Supplementary information

$MD_{fiber}(x,y)$	Fiber texture enhanced mass density map	$FF(MD(x,y))$ [1]
N_{pix}	Pixel number in cell mask	$\iint CM(x,y)\, dA$
OD	Optical density map (BF contrast)	$OD(x,y)$
$\underline{OD}$	Amplitude mean	$\iint_A OD(x,y)\, dxdy/N_{pix}$
$OD_{ent}(x,y)$	Entropy filtered optical density map	$\sum_{k=0}^{255} p_{OD,k} \cdot p_{OD,k}$
$\underline{OD_{STD,ker}}(x,y)$	Mean value of BF within STD filter kernel	$\int_{x-\frac{w_{STD}}{2}}^{x+\frac{w_{STD}}{2}} \int_{y-\frac{w_{STD}}{2}}^{y+\frac{w_{STD}}{2}} OD(u,v)\, dvdu \Big/ {w_{STD}}^2$
$OD_{STD}(x,y)$	BF STD map	$\int_{x-w_{STD}/2}^{x+w_{STD}/2} \int_{y-w_{STD}/2}^{y+w_{STD}/2} \sqrt{\frac{(OD(u,v)-\underline{OD_{STD,ker}}(x,y))^2}{{w_{STD}}^2}}\, dvdu$
$OD_{fiber}(x,y)$	Fiber texture enhanced optical density map	$FF(OD(x,y))$ [1]
P	Perimeter	$\oint_c \sqrt{\left(\left(\frac{dx}{d\theta}\right)^2+\left(\frac{dy}{d\theta}\right)^2\right)} d\theta$
$p_{MD,k}(x,y)$	Normalized histogram counts within kernel of mass density map	$\frac{number\ of\ pixels\ in\ kernel\ (w_{ent})\ with\ MD=k}{Total\ number\ of\ pixels\ in\ kernel}$, where k = 0 to 255
$p_{OD,k}(x,y)$	Normalized histogram counts within kernel of optical density map	$\frac{number\ of\ pixels\ in\ kernel\ (w_{ent})\ with\ OD=k}{Total\ number\ of\ pixels\ in\ kernel}$, where k = 0 to 255
r,θ	Polar coordinates centered at cell centroid	
w_{ent}	Kernel size of entropy filter	
w_{STD}	Kernel size of STD filter	
x,y	Cartesian coordinates	
x_{cen} y_{cen}	Coordinates of cell centroid	$x_{cen} = \iint_A x \cdot CM(x,y)\, dxdy/N_{pix}$ $y_{cen} = \iint_A y \cdot CM(x,y)\, dxdy/N_{pix}$

$x_{MD,cen}$ $y_{MD,cen}$	Coordinates of mass density weighted cell centroid	$x_{MD,cen} = \iint_A x \cdot MD(x,y)\, dxdy \,/\, N_{pix}$ $y_{MD,cen} = \iint_A y \cdot MD(x,y)\, dxdy \,/\, N_{pix}$
$x_{DMD,cen}$ $y_{DMD,cen}$	Coordinates of dry mass density weighted cell centroid	$x_{DMDcen} = \iint_A x \cdot DMD(x,y)\, dxdy / N_{pix}$ $y_{DMDcen} = \iint_A y \cdot DMD(x,y)\, dxdy / N_{pix}$
$x_{MDent,cen}$ $y_{MDent,cen}$	Coordinates of entropy filtered MD weighted cell centroid	$x_{MDent,cen} = \iint_A x \cdot MD_{ent}(x,y)\, dxdy / N_{pix}$ $y_{MDent,cen} = \iint_A y \cdot MD_{ent}(x,y)\, dxdy / N_{pix}$
$x_{MDfiber,cen}$ $y_{MDfiber,cen}$	Coordinates of fiber enhanced MD weighted cell centroid	$x_{MDfiber,cen} = \iint_A x \cdot MD_{fiber}(x,y)\, dxdy / N_{pix}$ $y_{MDfiber,cen} = \iint_A y \cdot MD_{fiber}(x,y)\, dxdy / N_{pix}$
$x_{MDfit,cen}$ $y_{MDfit,cen}$	Coordinates of MD fit texture weighted cell centroid	$x_{MDfit,cen} = \iint_A x \cdot MD_{fit}(x,y)\, dxdy / N_{pix}$ $y_{MDfit,cen} = \iint_A y \cdot MD_{fit}(x,y)\, dxdy / N_{pix}$
$x_{MDSTD,cen}$ $y_{MDSTD,cen}$	Coordinates of STD filtered MD weighted cell centroid	$x_{MDSTD,cen} = \iint_A x \cdot MD_{STD}(x,y)\, dxdy / N_{pix}$ $y_{MDSTD,cen} = \iint_A y \cdot MD_{STD}(x,y)\, dxdy / N_{pix}$
$x_{ODent,cen}$ $y_{ODent,cen}$	Coordinates of entropy filtered OD weighted cell centroid	$x_{ODent,cen} = \iint_A x \cdot OD_{ent}(x,y)\, dxdy / N_{pix}$ $y_{ODent,cen} = \iint_A y \cdot OD_{ent}(x,y)\, dxdy / N_{pix}$
$x_{ODfiber,cen}$ $y_{ODfiber,cen}$	Coordinates of fiber enhanced OD weighted cell centroid	$x_{ODfiber,cen} = \iint_A x \cdot OD_{fiber}(x,y)\, dxdy / N_{pix}$ $y_{ODfiber,cen} = \iint_A y \cdot OD_{fiber}(x,y)\, dxdy / N_{pix}$
$x_{ODSTD,cen}$ $y_{ODSTD,cen}$	Coordinates of STD filtered OD weighted cell centroid	$x_{ODSTD,cen} = \iint_A x \cdot OD_{STD}(x,y)\, dxdy / N_{pix}$ $y_{ODSTD,cen} = \iint_A y \cdot OD_{STD}(x,y)\, dxdy / N_{pix}$
α	Specific refractive increment	$0.19\ ml/g$ [2]
θ_{major}	Angle between major axis and x-axis	
F	Fourier transform	

Video S1: Evolution of cross-section particle distribution in HAR rectangular channel

Video S2: Evolution of cross-section particle distribution in HAR symmetric orifice channel

Video S3: Evolution of cross-section particle distribution in DIF system (HAR symmetric orifice channel then HAR rectangular channel)

Video S4: Evolution of cross-section particle distribution in revsered DIF system (HAR rectangular channel then HAR symmetric orifice channel)

For Video S1, S3, and S4, due to the significant size-dependency of inertial focusing, the time to focus particles of different sizes could vary more than 100 times. To better visualize the size-dependency of inertial focusing in a single and short video, we applied different video play speeds and color codes for each particle size and simultaneously played them.

Particle size (μm)	5	10	15	20	25
Color code	Red	Oragne	Green	Blue	Violet
Play speed	125x	64x	27x	8x	1x

Reference (Supplementary)

[1] H. Zhao, P. H. Brown, P. Schuck, *Biophys J* **2011**, *100*, 2309.
[2] A. F. Frangi, W. J. Niessen, K. L. Vincken, M. A. Viergever, in *Medical Image Computing and Computer-Assisted Intervention—MICCAI'98: First International Conference Cambridge, MA, USA, October 11–13, 1998 Proceedings 1*, Springer, **1998**, pp. 130–137.